Chinese Journal of Natural Medicines

Lirispirolides AL, a new class of sesquiterpene–monoterpene heterodimers with anti–neuroinflammatory activity from the rare medicinal plant *Liriodendron chinense*

Yuhang He, Kexin Li, Yufei Wu, Zexin Jin, Jinfeng Hu, Yicheng Mao, Juan Xiong

Citation: Yuhang He, Kexin Li, Yufei Wu, Zexin Jin, Jinfeng Hu, Yicheng Mao, Juan Xiong, Lirispirolides AL, a new class of sesquiterpene–monoterpene heterodimers with anti–neuroinflammatory activity from the rare medicinal plant *Liriodendron chinense*, Chinese Journal of Natural Medicines, 2025, 23(8), 938–950. doi: 10.1016/S1875–5364(25)60929–0.

View online: https://doi.org/10.1016/S1875–5364(25)60929–0

Chinese Journal of Natural Medicines 23 (2025) 938-950

Contents lists available at ScienceDirect

Chinese Journal of Natural Medicines

journal homepage: www.cjnmcpu.com/

Original article

Lirispirolides A–L, a new class of sesquiterpene-monoterpene heterodimers with anti-neuroinflammatory activity from the rare medicinal plant *Liriodendron chinense*

Yuhang He[a], Kexin Li[b], Yufei Wu[a], Zexin Jin[c], Jinfeng Hu[c,*], Yicheng Mao[b,*], Juan Xiong[a,*]

[a] *Department of Natural Medicine, School of Pharmacy, Fudan University, Shanghai 201203, China*
[b] *Department of Pharmacology, School of Pharmacy, Fudan University, Shanghai 201203, China*
[c] *Institute of Natural Medicine and Health Products, School of Pharmaceutical Sciences, Zhejiang Provincial Key Laboratory of Plant Evolutionary Ecology and Conservation, Taizhou University, Zhejiang 318000, China*

ARTICLE INFO

Article history:
Received 23 August 2024
Revised 3 November 2024
Accepted 16 January 2025
Available online 20 August 2025

Keywords:
Liriodendron chinense
Magnoliaceae
Lirispirolides
Sesquiterpene-monoterpene heterodimers
Anti-neuroinflammation

ABSTRACT

Lirispirolides A–L (**1**–**12**), twelve novel sesquiterpene-monoterpene heterodimers featuring distinctive carbon skeletons, were isolated from the branches and leaves of Chinese tulip tree [*Liriodendron chinense* (*L. chinense*)], a rare medicinal and ornamental plant endemic to China. The structural elucidation was accomplished through comprehensive spectroscopic analyses, quantum-chemical calculations, and X-ray crystallography. These heterodimers exhibit a characteristic 2-oxaspiro[4.5]decan-1-one structural motif, biosynthetically formed through intermolecular [4 + 2]-cycloaddition between a germacrane-type sesquiterpene and an ocimene-type monoterpene. The majority of the isolated compounds demonstrated significant anti-neuroinflammatory effects in lipopolysaccharide (LPS)-induced BV-2 microglial cells by reducing the production of pro-inflammatory mediators, specifically tumor necrosis factor-α (TNF-α) and nitric oxide (NO). Further investigation revealed that the lirispirolides' inhibition of NO release correlated with decreased messenger ribonucleic acid (mRNA) expression of inducible NO synthase (iNOS).

1. Introduction

The Magnoliaceae family represents one of the most ancient angiosperm populations, with origins dating to the Early Cretaceous period and extensive geological distribution [1]. Currently, this family encompasses over 300 species globally, distributed across temperate, subtropical, and tropical regions. China hosts approximately 120 endemic species, with South-west and South China serving as primary diversity centers [1]. These species are valued both as ornamental plants, prized for their aesthetic flowers and aromatic qualities, and as traditional Chinese medicinal resources, notably Cortex Magnoliae Officinalis (Houpo) and Flos Magnoliae (Xinyi) [1, 2]. However, the Magnoliaceae family faces significant conservation challenges due to limited population sizes and reduced reproductive capabilities. Recent assessments indicate that approximately 80% of Chinese Magnoliaceae species are under threat [3]. This situation has prompted increased focus on conservation and sustainable utilization efforts. Previous phytochemical studies of Magnoliaceae plants have revealed diverse terpenoid hybrids, including sesquiterpene-alkaloid heterodimers from *Magnolia grandiflora* [4] and *Liriodendron chinense* [5, 6], monoterpene-neolignan hetero-dimer/-trimers and monoterpene-polyketide-phenylpropane trimers from *Magnolia officinalis* var. *biloba* [7-10]. Additionally, researchers have identified bioconjugates of sesquiterpenes and neolignans connected through ether linkages [11, 12]. These terpenoid hybrids demonstrate diverse biological activities, including anti-inflammatory properties [4, 12], cytotoxic effects [5, 6], anti-diabetic potential [7, 9, 10], and neuroprotective capabilities [8, 10]. Such findings highlight the remarkable capacity of Magnoliaceae plants to produce complex hybrid natural products. These natural hybrids, characterized by intricate molecular structures and significant bioactivities, have garnered substantial attention in chemical and biological research communities [13-16]. Biosynthetically, these natural hybrids typically form through [4 + 2] Diels-Alder reaction, [2 + 2] cycloaddition, or Michael addition.

Liriodendron chinense (*L. chinense*), commonly known as Chinese tulip tree, is valued both as an ornamental species for its distinctive tulip-like flowers and unique leaf morphology, and as a traditional medicinal plant in China, historically used to treat cough and arthritis [17]. Currently, *L. chinense* faces significant conservation challenges [18, 19], being classified as a "near threatened (NT)" species by the International Union for Conservation of Nature (IUCN) Red List [19] and listed among China's National Secondary Protection species [20]. Previous research examining the alkaloid components of this plant identified several unique sesquiterpene-alkaloid heterocoupled dimers (liriogerphines A–U) [5, 6]. Continuing investigations into terpenoid hybrids from *L. chinense* focused on the non-alkaloid fraction of branches and leaves. Through high-performance liquid chromatography (HPLC)-prom-

* Corresponding author.
E-mail addresses: jfhu@tzc.edu.cn (J. Hu); maoyc@fudan.edu.cn (Y. Mao); jxiong@fudan.edu.cn (J. Xiong)

https://doi.org/10.1016/S1875-5364(25)60929-0

inence diode array (PDA)-mass spectrometry (MS)-guided isolation (Fig. S1), 12 novel sesquiterpene -monoterpene heterodimers were identified and characterized (Fig. 1). These heterodimers exhibit a distinctive 2-oxaspiro[4.5]decan-1-one structure, formed through [4 + 2]-cycloaddition between germacrane-type sesquiterpene and ocimene-type monoterpene components. This paper presents their isolation, structural characterization, proposed biosynthetic pathway, and anti-neuroinflammatory properties. This work is Part XXXV in a series of "Phytochemical and biological studies on rare and endangered plants endemic to China" (for Part XXXIV, see ref. [21]).

2. Results and discussion

Lirispirolide A (**1**) was isolated as colorless crystals in MeOH. The molecular formula was determined to be $C_{27}H_{38}O_7$ based on the (+)-high-resolution electrospray ionization MS (HR-ESI-MS) ion at *m/z* 497.2513 [M + Na]$^+$ (Calcd. for $C_{27}H_{38}O_7Na^+$, *m/z* 497.2510) and the ^{13}C nuclear magnetic resonance (NMR) data, indicating nine indices of hydrogen deficiency (IHDs). The ^{1}H NMR spectrum of **1** revealed proton resonances for six methyls, including three tertiary methyls [δ_H 1.32 (s, Me-9'), 1.33 (s, Me-15), 1.39 (s, Me-8')], two vinyl methyls [δ_H 1.63 (d, J = 1.1 Hz, Me-10'), 1.69 (br s, Me-14)], and one acetyl methyl at δ_H 2.09 (s, 8-OAc). Additionally, three oxymethine protons [δ_H 2.67 (H-5), 4.37 (H-6), 5.27 (H-8)] and four olefinic protons [δ_H 5.34 (H-1), 5.54 (H-5'), 5.61 (H-2'), 5.73 (H-6')] were observed (Table 1). The ^{13}C and heteronuclear single quantum correlation (HSQC) NMR spectra identified 27 carbon signals (Table 1) categorized as two carbonyls (one lactone group at δ_C 174.6 and one acetyl at δ_C 169.4), six olefinic carbons (comprising two trisubstituted and one disubstituted double bonds), three non-proton-bearing sp^3 carbons (two oxygenated at δ_C 82.0 and 61.7), five sp^3 methines (three oxygenated at δ_C 75.7, 70.8, and 67.8), five sp^3 methylenes, and six methyls. In conjunction with the known chemical substance profile of Chinese tulip tree [22], these findings suggested that **1** might be a hetero-adduct consisting of a sesquiterpene unit (unit A) and a monoterpene unit (unit B). In subunit A, three spin systems corresponding to H-1/H_2-2/H_2-3, H-5/H-6/H-7, and H-8/H_2-9 were identified in the ^{1}H–^{1}H correlation spectroscopy (COSY) spectrum (Fig. 2). Combined with the heteronuclear multiple bond correlation (HMBC) of H-6 with C-8/C-11/C-12, of H-7 with C-9/C-13, of H-8 with C-11 and the acetoxyl carbonyl carbon, of H_3-14 with C-1/C-9/C-10, and of H_3-15 with C-3/C-4/C-5, unit A was determined to be a germacrane-type sesquiterpenolide highly similar to lipiferolide, previously reported from the title plant [22,23]. The remaining ten carbons assigned to unit B were established by the ^{1}H–^{1}H COSY correlations of H_2-1'/H-2' and H-4'/H-5'/H-6', and the HMBC of H_3-10' with C-2'/C-3'/C-4', of H-5' with C-3'/C-7', and of H_3-8'/H_3-9' with C-6'/C-7'. These correlations established unit B as a monoterpene featuring the myrc-2',5'-diene framework with C-7' being oxygenated. Notably, compared to 7-hydroxy-myrcene, the chemical shift of C-7' exhibited a downfield shift from δ_C 70.9 [24] to 82.0 in **1**, indicating the presence of a unique peroxide group at C-7' [25]. Consistent with this, the molecular formula of **1** contained seven oxygen atoms, with five attributed to unit A and two to the 7'-substituent in unit B. The two units were connected *via* the newly formed C-13–C-1' and C-11–C-4' bonds, evidenced by the diagnostic ^{1}H–^{1}H COSY correlation of H_2-13/H_2-1' and the HMBC of H-7/C-4', H_2-13/C-4', H-1'b/C-11, and H-4'/C-12 (Fig. 2), as well as the unsaturation requirement. Therefore, compound **1** was characterized as a germacrane-myrcane heterodimer featuring a unique 2-oxaspiro [4.5]decan-1-one motif.

The relative configuration of **1** was determined through analysis of the rotating-frame Overhauser effect spectroscopy (ROESY) spectrum and key proton-proton coupling constants (Table 1). In unit A, the ROE correlations (Fig. 2) of H-5/H-7, H-7/H-9α, H-6/H_3-15, H_3-14/H_3-15, combined with the large *trans*-diaxial coupling constants (9.4 or 9.3 Hz) within the H-5/H-6/H-7 system, and the small coupling constant (near zero) between H-8 and H-7, confirmed that the relative configuration of the sesquiterpene unit aligned with lipiferolide and its analogs [23]. The large magnitude of $J_{H\text{-}5',6'}$ (15.8 Hz) established the *E*-configuration of the C-5'/C-6' double bond. Regarding the relative configuration of the newly formed spirocyclic ring, the ROE correlation of H-13b/H-6 indicated the C-11–C-13 bond to be β-oriented (i.e., C-11 to be S^*-configured), while the ROE correlation of H-4'/H-8 demonstrated their α-orientations. The absolute configuration of **1** was verified through electronic circular dichroism (ECD) calculation using time-dependent density functional theory (TD-DFT) [26]. As illustrated in Fig. 3A, the calculated ECD curve of (4*R*,5*S*,6*S*,7*R*,8*R*,11*S*,4'*R*)-**1** corresponded to the experimental data. Subsequently, suitable crystals of **1** were obtained in MeOH, and a single-crystal X-ray diffraction experiment (Ga Kα) was conducted [Fig. 4, Flack parameter = 0.03 (4)], definitively confirming the previous structural assignments.

Lirispirolides B (**2**) and C (**3**) shared the same molecular formula of $C_{27}H_{38}O_7$ as **1**, as determined by HR-ESI-MS and ^{13}C NMR data. Their 1D NMR data exhibited strong similarities to those of **1**, with primary differences observed at C-11 (δ_C 50.6 in **1**; δ_C 48.6 in **2**; δ_C 50.0 in **3**), C-4' (δ_C 47.5 in **1**; δ_C 48.8 in **2**; δ_C 43.5 in **3**), and their adjacent groups. Analysis of their HMBC spectra revealed a planar structure identical to **1**, suggesting these compounds might be epimers with distinct configurations at the newly formed chiral centers C-11 and C-4'. Comparative analysis of their ^{1}H–^{1}H coupling constants and ROESY spectra confirmed that the relative configuration of unit A in both **2** and **3** was identical to that of **1** (Fig. 2). Regarding the stereochemistry of C-11 and C-4', the ROE correlation of H_2-13 with H-6 in **2** established the 11S^*-configuration, indicating compound **2** as the 4'-epimer of **1**. For compound **3**, the ROE correlation of H_2-13 with H-7 instead of H-6 indicated a different configuration at C-11 (11R^*-configuration), though the relative configuration of C-4' remained challenging to determine due to insufficient evidence from ROESY data and coupling constant. ECD calculations were performed for all four possible isomers (Fig. S2, Supporting information). The results indicated that the $\Delta^{2'}$ and $\Delta^{5'}$ groups primarily contributed to the Cotton effect (CE) around 200 nm. The calculated ECD curves of 11*S*,4'*S*- and 11*R*,4'*S*-isomers showed a positive CE around 200 nm, while the 4'*R*-isomers displayed negative ones. Consequently, the C-4' configurations in **2** and **3** were both determined as *S* based on their similar positive CE around 200 nm in their ECD spectra (Fig. 3B). Therefore, the

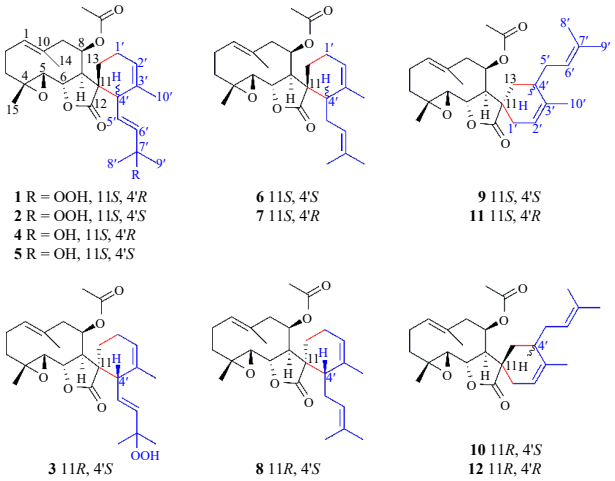

Fig. 1 Structures of compounds **1**–**12** from *L. chinense*.

Table 1 ^{1}H (600 MHz) and ^{13}C (150 MHz) NMR data for **1**–**3** (J in Hz, $CDCl_3$).

No.	**1**		**2**		**3**	
	δ_C	δ_H, mult.	δ_C	δ_H, mult.	δ_C	δ_H, mult.
1	128.1	5.34, br d (11.8)	128.2	5.33, br d (11.8)	127.9	5.34, br d (12.0)
2α	23.9	2.21, m	23.9	2.25, m	23.8	2.27, m
2β		2.40, dddd (13.0, 12.8, 11.8, 6.1)		2.41, m		2.41, m
3α	36.5	1.23, ddd (13.1, 12.8, 7.1)	36.4	1.29, m	36.3	1.29, m
3β		2.14, ddd (13.1, 6.1, 1.1)		2.17, br dd (13.0, 6.2)		2.17, ddd (13.0, 6.2, 1.1)
4	61.7		61.9		62.0	
5	67.8	2.67, d (9.3)	68.0	2.74, d (9.3)	68.2	2.70, d (9.1)
6	75.7	4.37, dd (9.4, 9.3)	74.9	4.39, dd (9.3, 9.2)	75.8	4.56, dd (9.2, 9.1)
7	49.5	2.93, br d (9.4)	53.0	2.55, br d (9.2)	55.8	2.44, br d (9.2)
8	70.8	5.27, br d (6.1)	71.3	5.54, br d (6.2)	71.7	5.61, br d (6.2)
9α	43.8	2.16, br d (14.0)	42.9	2.26, m	43.8	2.10, m
9β		2.81, dd (14.0, 6.1)		2.62, dd (14.0, 6.2)		2.88, dd (14.2, 6.2)
10	130.5		130.7		130.8	
11	50.6		48.6		50.0	
12	174.6		176.0		178.4	
13a	23.6	1.72, br dd (13.0, 5.0)	19.4	1.63, m	28.3	2.22, ddd (13.9, 11.7, 6.1)
13b		1.50, ddd (13.0, 12.5, 5.2)		1.55, m		1.56, m
14	20.0	1.69, br s	19.9	1.67, br s	20.2	1.68, br s
15	16.6	1.33, s	16.6	1.34, s	16.8	1.36, s
8-OAc	21.2	2.09, s	21.3	2.08, s	21.4	2.12, s
	169.4		169.6		169.1	
1'a	21.7	2.21, m	22.6	2.12, m	21.7	2.42, m
1'b		2.03, br d (15.2)		2.11, m		1.99, m
2'	122.6	5.61, br d (5.0)	122.2	5.59, br s	123.2	5.68, br s
3'	131.4		131.6		133.0	
4'	47.5	2.64, br d (10.2)	48.8	2.64, br d (8.0)	43.5	2.53, br d (9.5)
5'	128.7	5.54, dd (15.8, 10.2)	127.8	5.60, dd (15.9, 8.0)	130.6	5.62, dd (15.7, 9.6)
6'	141.2	5.73, br d (15.8)	139.0	5.78, br d (15.9)	136.8	5.44, br d (15.7)
7'	82.0		81.6		81.3	
8'	23.3	1.39, s	23.8	1.41, s	25.1	1.33, s
9'	24.9	1.32, s	24.7	1.38, s	25.3	1.30, s
10'	22.6	1.63, d (1.1)	22.3	1.64, br s	22.6	1.56, d (1.2)
7'-OOH						8.38, s

absolute configurations of lirispirolides B (**2**) and C (**3**) were established as (4*R*,5*S*,6*S*,7*R*,8*R*,11*S*,4'*S*) and (4*R*,5*S*,6*S*,7*R*,8*R*,11*R*,4'*S*), respectively.

Lirispirolides D (**4**) and E (**5**) share the chemical formula $C_{27}H_{38}O_6$, as determined by HR-ESI-MS and ^{13}C NMR data, containing one less oxygen atom than compounds **1**–**3**. Analysis of their 1D NMR data (Table 2) confirmed the heterodimeric skeleton. Unlike compounds **1**–**3**, which feature a 7'-OOH group, compounds **4** and **5** contain a hydroxy group at C-7', evidenced by the upfield shifted carbon signal of C-7' (δ_C 70.6 in **4** and **5**; δ_C > 80 in **1**–**3**) and their molecular formula. Regarding the stereochemistry of **4**, the NMR data closely matched that of **1**, particularly around C-11 and C-4', indicating identical relative configuration. Similarly, compound **5** showed nearly identical 1D NMR data to **2**, suggesting the same configuration. ECD spectra comparison confirmed these assignments, establishing the absolute configurations of **4** and **5** as (4*R*,5*S*,6*S*,7*R*,8*R*,11*S*,4′*R*) and (4*R*,5*S*,6*S*,7*R*,8*R*,11*S*,4′*S*), respectively (Fig. 3B).

The (+)-HR-ESI-MS and ^{13}C NMR data of lirispirolide (**6**) indicated a molecular formula of $C_{27}H_{38}O_5$. Examination of its 1D NMR data (Tables 3 and 4) and characteristic molecular weight suggested a similar sesquiterpene -monoterpene heterodimeric skeleton. Compared to compounds **1**–**5**, compound **6** lacked an oxygenated group at C-7'. Additionally, the two tertiary methyls

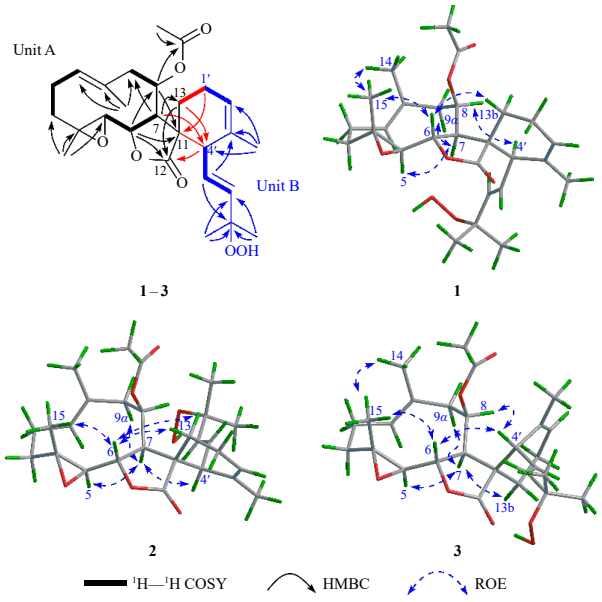

Fig. 2 Selected COSY (bold bonds), HMBC, and ROESY correlations of **1**–**3**.

of Me-8' and Me-9' were replaced by vinyl groups [δ_H 1.66 (3H, br s), 1.76 (3H, br s)], while the *trans*-configured C-5'–C-6' double bond signals were absent, indicating a shift of the $\Delta^{5'}$ double bond to C-6'–C-7'. HMBC of H_3-8'/H_3-9' with C-6' and C-7', and of H_2-5' with C-7' confirmed this structure (Fig. 5). The relative configuration matched that of **2** based on comparable 1D NMR and ROESY data (Fig. 5). ROE correlations between H-6 and H-13b, and H-8 with H_2-5' confirmed the 11S^*,4'S^*-configuration. The experimental and calculated ECD curves showed agreement (Fig. 6A), both exhibiting a positive CE around 210 nm and a negative one around 230 nm, establishing the absolute configuration of **6** as (4*R*,5*S*,6*S*,7*R*,8*R*,11*S*,4'*S*). Single-crystal X-ray diffraction analysis using Cu Kα radiation [Fig. 7, Flack parameter = 0.07 (17)] provided final confirmation of these structural assignments.

Lirispirolides G (**7**) and H (**8**) share the same elemental composition, $C_{27}H_{38}O_5$, as **6**, as confirmed by (+)-HR-ESI-MS and ^{13}C NMR data. Analysis of their 1D NMR data (Tables 3 and 4) and HMBC (Fig. 5) revealed that **7** and **8** possess identical planar structures to **6**, differing only in stereochemistry at the [4 + 2]-cyclohexene ring. The ROESY spectrum of **7** showed a ROE correlation between H-6 and H-13a, indicating the β-orientation of CH_2-13 (C-11 being S^*-configured), while the ROE correlation between H-4' and H-8 indicated the α-orientation of H-4' (C-4' being R^*-configured). The ECD spectrum of **7** (Fig. S3) displayed a negative CE around 200 nm, contrasting with the positive CE in **6**, enabling the assignment of C-4' absolute configuration as *R*. Consequently, the complete absolute configuration of **7** was established as (4*R*,5*S*,6*S*,7*R*,8*R*,11*S*,4'*R*). For compound **8**, C-11 stereochemistry was determined as R^* based on ROE correlations of H-7/H-13b, H-6/H-4', and H-6/H-5'b. Similar to compound **3**, C-4' configuration remained ambiguous due to inconclusive ROESY data. Theoretical ^{1}H and ^{13}C NMR chemical shifts for both possible 4'-isomers of **8** were calculated at PCM/b3lyp/6-31g(d) level [27,28]. The results (Fig. 8) showed that the calculated ^{13}C NMR data of 4'S^*-**8** (**8a**) showed excellent correlation with experimental data, exhibiting a high correlation coefficient (R^2) of 0.9990, lower corrected mean absolute error (CMAE), and 100% DP4+ probability [DP4+ (all (H and C) data)]. These findings confirmed the 4'S^*-configuration of **8**. ECD calculations on **8a** and **8b** further validated C-4' stereochemistry, with the calculated ECD curve of (11*R*,4'*S*)-isomer (**8a**) closely matching experimental data (Fig. 6B). Thus, the absolute configuration of **8** was determined as (4*R*,5*S*,6*S*,7*R*,8*R*,11*R*,4'*S*).

Lirispirolide I (**9**) was isolated as colorless crystals in MeOH. The (+)-HR-ESI-MS and ^{13}C NMR data established its molecular formula as $C_{27}H_{38}O_5$, identical to that of lirispirolides F–H (**6**–**8**). The ^{1}H and ^{13}C NMR spectral data (Tables 3 and 5) showed close similarity to those of **6**–**8**, with primary differences observed in the [4 + 2]-cyclohexene ring region (C-11–C-13 and C-1'–C-5'). The identical units A and B in **9** were confirmed through comparable 1D NMR data and HMBC (Fig. 9). The $^3J_{H,C}$ HMBC cross-peaks of H-7 with C-1', of H_2-13 with C-1' and C-5', of H-1a' with C-12, and of H-2' with C-11 (Fig. 9) connected units A and B *via* two linkage bonds of C-13–C-4' and C-11–C-1', revealing a distinct cyclohexene ring structure compared to lirispirolides A–H. The relative configuration of this novel ring in **9** was determined through ROESY analysis. As shown in Fig. 9, the ROE correlations of H-6/H-1'b and H-7/H_2-13 indicated an α-oriented C-11–C-13 bond (i.e., C-11 with S^* configuration), while the ROE correlation of H-8/H-4' confirmed the α-orientation of H-4' (i.e., C-4' with S^* configuration). X-ray crystallographic analysis (Ga Kα) of **9**, with a Flack parameter of 0.04 (14), validated the structural assignment based on NMR data and established its absolute configuration as 4*R*,5*S*,6*S*,7*R*,8*R*,11*S*,4'*S* (Fig. 10).

Lirispirolides J–L (**10**–**12**) share the same molecular formula ($C_{27}H_{38}O_5$) with **9** and exhibit highly similar 1D NMR data (Tables 3 and 5). Analysis of their ^{1}H–^{1}H COSY, HSQC, and HMBC spectra (Figs. 9, S70, S75, S76, and S83–85) confirmed their identical planar structure, indicating that **10**–**12** are regioisomers of **9** with varying configurations at C-11 and C-4'. Regarding the relative configuration of C-11, similar to **9**, the distinct ROE cross-peak between H-7 and H_2-13 in the ROESY spectrum of **11** established the 11S^*-configuration. The ROE correlation between H-7 and H_2-1' in both **10** and **12** confirmed their 11R^*-configuration (Fig. 9). However, determining the C-4' configuration in compounds **10**–**12** proved challenging due to inconclusive ROESY data and *J*-based configuration analysis. To resolve this uncertainty, TD-DFT-ECD calculations were performed on all four possible 11,4'-isomers. As shown in Fig. 11, the two 4'*S*-isomers (**9** and **10**) exhibited negative CEs around 200 nm in both calculated and experimental ECD spectra. Conversely, the calculated and experimental ECD curves of the two 4'*R*-isomers (**11** and **12**) showed positive CEs in the 200–230 nm range. Supporting this finding, the Ga Kα X-ray diffraction analysis of **10** [Fig. 10, Flack parameter = 0.04 (17)] definitively established its absolute configuration as 4*R*,5*S*,6*S*,7*R*,8*R*,11*R*,4'*S*. Consequently, the absolute

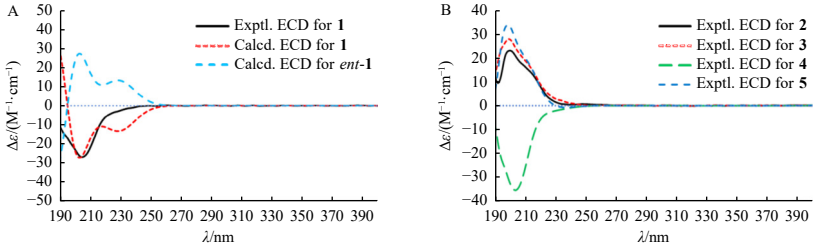

Fig. 3 (A) Experimental and calculated ECD spectra of **1**; (B) Experimental ECD spectra of **2**–**5**.

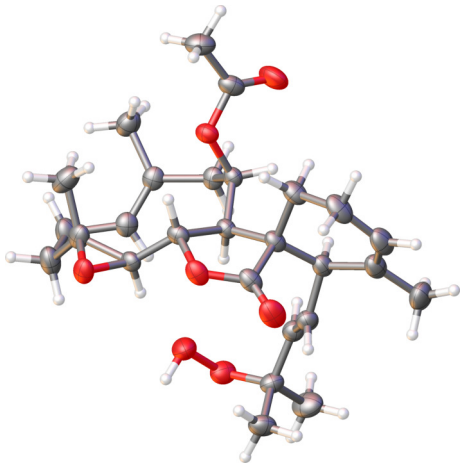

Fig. 4 Olex2 drawing of **1**.

configurations of **11** and **12** were determined as (4*R*,5*S*,6*S*,7*R*,8*R*,11*S*,4'*R*) and (4*R*,5*S*,6*S*,7*R*,8*R*,11*R*,4'*R*), respectively.

Lirispirolides A–L (**1**–**12**) constitute a unique class of sesquiterpene-monoterpene heterodimers with novel carbon skeletons. These compounds likely originate through an intermolecular [4 + 2] DA cycloaddition between germacranolide-type sesquiterpene and ocimene-type monoterpene components (Scheme 1). The exocyclic group of lipiferolide, a predominant constituent in the title plant, functions as the electron-deficient "dienophile", while the conjugated 1,3-diene group in ocimene monoterpenes (e.g., *β*-ocimene) serves as the "diene" in the DA reaction. In compounds **1**–**8**, the two units connect *via* newly formed C-11–C-4' and C-13–C-1' bonds. For compounds **9**–**12**, the units conjugate *via* C-11–C-1' and C-13–C-4' bonds. These distinct assembly modes generate 1,4- and 4,1-adducts, representing two subtypes of germacrene-ocimene heterodimers with distinctive spirocyclic carbon skeletons. Notably, no *exo*-/*endo*-stereoselectivity was observed during DA cycloaddition product formation. This is exemplified by compounds **9**–**12**, where all four possible isomers of [4 + 2]-dimerization from identical precursors were isolated.

Numerous naturally occurring homo- or heterodimeric terpenes have been reported, garnering significant attention due to their complex structures, diverse bioactivities, and synthetic challenges [16, 28–35]. Within this group, sesquiterpene-monoterpene hybrids represent a relatively small subset [16, 29, 31–35]. Notably, heterodimers formed between germacrene-type sesquiterpenoids and myrcane-type monoterpenoids are particularly rare in nature, with only two documented examples: caleamyrcenolide [36] from *Calea hymenolepis* and genepolide [37] from *Artemisia umbelliformis*. When genepolide was initially reported in 2009, researchers emphasized its significance as a genuine natural product with an interesting structural motif warranting systematic investigation [37]. This type of naturally occurring sesquiterpene-monoterpene hybrid remained undiscovered for approximately fifteen years until the present study. From a biogenetic perspective, both caleamyrcenolide and genepolide (detailed in Scheme S1 in Supporting information) utilize the 1,3(10)-diene group of the myrcene unit as the "diene" component in the DA reaction, whereas in lirispirolides A–L, the "diene" component originates from the 1,3-diene group of the ocimene unit (Scheme 1). The discovery and verification of naturally occurring Diels-Alderase in plants catalyzing intermolecular DA transformations [38] provides compelling evidence that these natural DA adducts are genuine natural products rather than isolated artifacts.

Neuroinflammation has been established as a significant factor in the pathology of ischemic stroke, Parkinson's disease (PD), Alzheimer's disease (AD), and depression [39–41]. Inhibiting the overactivation of microglia, the resident immune cells of the central nervous system, by suppressing the expression and release of pro-inflammatory mediators such as nitric oxide (NO), tumor necrosis factor-α (TNF-α), and interleukin-6 (IL-6) has emerged as a promising therapeutic strategy for the treatment of neurological disorders [42]. The title plant, traditionally used in Chinese medicine for treating arthritis, demonstrates the potential for neuroinflammation modulation. Consequently, all isolates were evaluated *in vitro* for anti-neuroinflammatory effects by measuring NO production inhibition in lipopolysaccharide (LPS)-induced mouse BV-2 microglial cells. As indicated in Table 6, nearly all heterodimers (excluding **1**) demonstrated significant NO level reduction [half maximal inhibitory concentration (IC_{50})

Table 2 ^{1}H and ^{13}C NMR data of **4** and **5** (*J* in Hz, $CDCl_3$).

No.	**4**		**5**	
	δ_C [a]	δ_H [b], mult.	δ_C [a]	δ_H [c], mult.
1	127.9	5.24, m	128.1	5.31, br d (11.6)
2*α*	23.8	2.21, m	23.9	2.25, br d (14.1)
2*β*		2.40, m		2.40, m
3*α*	36.4	1.25, ddd (13.1, 13.0, 6.6)	36.4	1.26, ddd (12.9, 12.9, 6.8)
3*β*		2.15, br dd (13.1, 6.5)		2.15, br dd (12.9, 6.2)
4	61.7		61.9	
5	68.1	2.61, d (9.2)	68.0	2.58, d (9.3)
6	75.5	4.36, dd (9.5, 9.2)	74.6	4.37, dd (9.3, 9.2)
7	49.9	2.76, br d (9.5)	52.9	2.73, br d (9.2)
8	70.6	5.24, br d (6.2)	71.1	5.47, br d (6.4)
9*α*	44.0	2.04, m	42.7	2.23, m
9*β*		2.81, dd (14.2, 6.2)		2.62, dd (14.1, 6.4)
10	130.7		130.7	
11	50.5		48.6	
12	174.5		176.1	
13a	23.6	1.70, m	19.3	1.61, m
13b		1.47, ddd (12.7, 12.5, 5.3)		1.53, m
14	20.0	1.69, br s	19.9	1.65, br s
15	16.6	1.32, s	16.6	1.32, s
8-OAc	21.2	2.09, s	21.2	2.06, s
	169.3		169.3	
1'a	21.6	2.18, m	22.6	2.10, m
1′b		2.01, m		2.08, m
2'	122.5	5.58, br d (4.5)	121.8	5.54, br s
3'	131.6		131.7	
4'	47.1	2.58, br d (10.2)	48.9	2.54, br d (9.0)
5'	124.7	5.50, dd (15.7, 10.2)	124.3	5.53, dd (15.6, 9.0)
6'	145.5	5.76, br d (15.7)	142.5	5.75, br d (15.6)
7'	70.6		70.6	
8'	29.9	1.36, s	30.0	1.38, s
9'	29.9	1.35, s	29.5	1.36, s
10'	22.7	1.61, br s	22.3	1.62, br s

[a] acquired in 150 MHz; [b] acquired in 600 MHz; [c] acquired in 400 MHz.

Table 3 ^{13}C NMR (150 MHz) data for **6**–**12**.

No.	**6** [a]	**7** [a]	**8** [a]	**9** [a]	**10** [a]	**11** [a]	**12** [a]	**12** [b]
1	128.2	127.9	127.7	128.0	128.0	128.0	128.1	128.3
2	24.0	23.9	23.7	24.0	23.8	23.8	23.8	24.0
3	36.5	36.6	36.4	36.2	36.5	36.5	36.4	36.9
4	61.9	61.5	61.8	61.9	61.7	61.7	61.7	61.8
5	68.2	68.0	68.5	68.0	67.7	68.0	67.9	67.9
6	74.3	75.4	75.3	75.2	75.5	75.4	75.4	76.2
7	52.9	51.2	56.6	55.0	54.6	55.4	55.7	55.4
8	71.5	71.1	71.7	72.2	70.9	71.0	71.8	72.1
9	43.5	44.0	43.8	44.0	43.9	43.7	43.7	43.6
10	130.9	130.9	130.9	131.2	130.8	130.7	130.8	130.9
11	49.8	51.5	48.6	45.7	45.9	45.3	44.7	45.1
12	176.8	175.3	177.7	180.3	177.1	176.6	179.3	179.9
13	20.7	24.7	29.4	39.0	29.7	35.5	28.8	29.4
14	19.9	20.0	20.2	20.0	20.0	20.0	20.0	19.9
15	16.7	16.6	16.8	16.8	16.6	16.6	16.7	16.7
8-OAc	21.3	21.3	21.3	21.2	21.0	21.1	21.3	21.1
	169.1	169.4	169.2	169.1	168.9	169.4	169.5	169.9
1'	22.5	21.3	21.9	28.8	31.4	27.2	32.9	32.7
2'	122.0	123.1	123.1	120.7	119.0	116.7	118.5	119.7
3'	133.2	134.3	135.3	136.8	136.9	137.6	136.8	136.4
4'	44.3	42.6	40.1	35.4	35.2	35.7	37.6	37.9
5'	27.8	28.2	29.3	30.7	30.7	31.1	30.6	31.1
6'	121.0	125.7	122.5	120.9	122.0	121.7	122.5	123.2
7'	133.5	132.2	132.8	133.8	132.8	133.2	133.4	133.0
8'	18.6	18.1	18.1	18.0	17.9	18.1	17.9	17.8
9'	25.7	26.0	25.9	25.9	25.8	25.9	25.8	25.7
10'	22.7	22.4	22.9	21.0	21.1	21.3	21.8	21.9

[a] acquired in $CDCl_3$; [b] acquired in pyridine-d_5.

values ranging from 10.84 to 48.14 μmol·L^{-1})] while maintaining acceptable cytotoxicity levels against microglial cells at 50 μmol·L^{-1} (cell viability ≥ 70.0%). Compound **10** exhibited optimal activity (IC_{50} 10.84 ± 1.78 μmol·L^{-1}) with minimal cytotoxicity (cell viabilities ≥ 95.0% at 50 μmol·L^{-1}). Notably, compounds **1**–**12** showed no significant anti-leukemia activity (data not shown), distinguishing them from previously isolated sesquiterpene-alkaloid heterodimers from the same plant [5, 6].

Additionally, the effects of lirispirolides on pro-inflammatory cytokine production (TNF-α and IL-6) and inducible NO synthase (*iNOS*) messenger ribonucleic acid (mRNA) expression were examined in LPS-induced BV-2 cells. Compound **9** demonstrated a notable reduction in TNF-α release (Fig. 12A), surpassing the positive control's effectiveness. The other heterodimers showed moderate to weak inhibitory effects on TNF-α secretion (Fig. 12A). However, none exhibited significant IL-6 expression inhibition (Fig. 12B). Most heterodimers (except **4** and **9**) significantly reduced *iNOS* mRNA levels (Fig. 12C) in over-activated BV-2 cells, suggesting that NO production suppression by lirispirolides correlates with *iNOS* mRNA expression attenuation.

Rare and endangered plants (REPs), particularly medicinal species, represent a valuable resource for the discovery of natural therapeutic compounds [43, 44]. This investigation of the non-alkaloid fraction of the rare medicinal plant Chinese tulip tree (*L. chinense*), guided by LC-PDA-MS analysis, resulted in the isolation and characterization of 12 novel sesquiterpene-monoterpene heterodimers (lirispirolides A–L, **1**–**12**). These heterodimers, formed through [4 + 2] cycloaddition bioconjugation, exhibit a distinctive germacranolide-ocimene heterocoupled skeleton with a spirocyclic ring system. The compounds demonstrated significant inhibition of LPS-induced NO production by suppressing iNOS transcriptional levels in BV-2 microglial cells. These findings highlight the therapeutic potential of these heterodimers for treating neuroinflammation-related cerebral diseases and encourage further investigation of the relict Chinese tulip tree.

3. Experimental

3.1. General experimental procedures

Optical rotations were measured using a Rudolph Autopol IV automatic polarimeter (Rudolph Research Analytical, Hackett-

Table 4 ^{1}H NMR (600 MHz) data of **6–8** (J in Hz, $CDCl_3$).

No.	6	7	8
1	5.33, br d (11.8)	5.28, br d (11.9)	5.33, br dd (11.8, 3.2)
2α	2.24, m	2.24, m	2.23, m
2β	2.41, m	2.42, dddd (12.9, 12.8, 11.9, 6.1)	2.40, m
3α	1.28, ddd (13.0, 11.7, 6.6)	1.27, ddd (13.0, 12.8, 6.8)	1.29, ddd (12.9, 12.6, 7.2)
3β	2.18, br dd (13.0, 5.6)	2.17, ddd (13.0, 6.1, 1.1)	2.17, m
5	2.72, d (9.1)	2.65, d (9.3)	2.70, d (9.2)
6	4.41, dd (9.2, 9.1)	4.36, dd (9.4, 9.3)	4.45, dd (9.3, 9.2)
7	2.59, br d (9.2)	2.99, br d (9.4)	2.34, br d (9.3)
8	5.50, br d (6.5)	5.25, br d (6.3)	5.60, br d (6.3)
9α	2.24, m	2.06, br d (14.1)	2.07, m
9β	2.72, dd (14.0, 6.5)	2.82, dd (14.1, 6.3)	2.88, dd (14.2, 6.3)
13a	1.71, m	1.64, br dd (12.6, 4.5)	2.20, m
13b	1.54, ddd (13.4, 6.1, 2.4)	1.43, ddd (12.6, 12.5, 4.9)	1.51, br dd (14.1, 5.6)
14	1.68, br s	1.69, br s	1.66, br s
15	1.34, s	1.33, s	1.36, s
8-OAc	2.06, s	2.08, s	2.07, s
1'a	2.10, m	2.16, m	2.35, m
1'b	2.08, m	1.93, br d (16.8)	1.92, m
2'	5.56, br s	5.53, br d (5.9)	5.61, br s
4'	2.23, m	2.09, m	2.00, br d (6.7)
5'a	2.40, m	2.47, m	2.31, m
5'b	2.17, m	2.23, m	2.14, m
6'	5.20, br dd (6.0, 6.0)	5.18, br dd (7.2, 7.2)	5.02, br dd (6.7, 6.5)
8'	1.66, br s	1.67, br s	1.58, br s
9'	1.76, br s	1.75, br s	1.67, br s
10'	1.72, br s	1.73, d (1.1)	1.66, br s

stown, NJ, USA). Melting points were determined on an SGW X-4 Micro Melting Point Apparatus (Shanghai INESA Physico-Optical Instrument Co., Ltd., Shanghai, China). UV and IR spectra were obtained using a Hitachi U -2900E (Hitachi High-Tech Corporation, Tokyo, Japan) and a Thermo Scientific Nicolet iS5 FTIR spectrometer (Nicolet, Madison, WI, USA), respectively. ECD spectra were recorded using a JASCO J-810 spectropolarimeter (JASCO Corporation, Tokyo, Japan). NMR spectra were acquired on a Bruker Avance III 400 or 600 MHz spectrometer (Bruker, Rheinstetten, Germany). Chemical shifts are expressed in δ and referenced to the residual solvent signals. HR-ESI-MS were obtained on an AB SCIEX Q-TOF 5600 spectrometer (SCIEX, Framingham, MA, USA). X-ray crystallography was performed using a Bruker Apex Duo diffractometer (Bruker AXS Inc., Madison, WI, USA) equipped with graphite-monochromated Ga Kα radiation (λ = 1.341 39 Å) or Cu Kα radiation (λ = 1.541 78 Å). Semi-preparative HPLC was conducted using a Shimadzu LC-20AT system with an SPD-M20A PDA detector (Shimadzu Corporation, Kyoto, Japan) or on a Waters e2695 system with a 2998 PDA detector (Waters Corporation, Milford, MA, USA). Semi-preparative RP-HPLC columns (XBridge: 250 mm × 10 mm, 5 μm, Waters Corporation, Milford, MA, USA; Cosmosil: 250 mm × 10 mm, 5 μm, Shiseido Co., Ltd., Tokyo, Japan; Zorbax SB-Phenyl: 250 mm × 10 mm, 5 μm, Agilent Technologies, New Castle, DE, USA; Sunfire: 250 mm × 10 mm, 5 μm, Waters Corporation, Milford, MA, USA) were utilized for isolation. Column chromatography (CC) was performed using MCI gel CHP20P (75–150 μm, Mitsubishi Chemical Corporation, Tokyo, Japan), silica gel (100–200 or 200–300 mesh, Qingdao Marine Chemical Co., Ltd., Qingdao, China), and Sephadex LH -20 (GE Healthcare Bio-Sciences AB, Uppsala, Sweden). Gel-precoated plates (GF_{254}, 0.25 mm, Yantai Jiangyou Silica Gel Development Co., Ltd., Yantai, China) were employed for TLC detection. Spots were visualized under UV light (254 nm) and through spraying with 10% (V/V) sulfuric acid/ethanol solution containing 1% vanillin followed by heating to 120 °C. All solvents used in this study were of either analytical reagent grade (China National Pharmaceutical Group Co., Ltd., Shanghai, China) or HPLC grade purity (Sigma-Aldrich Corporation, St. Louis, MO, USA).

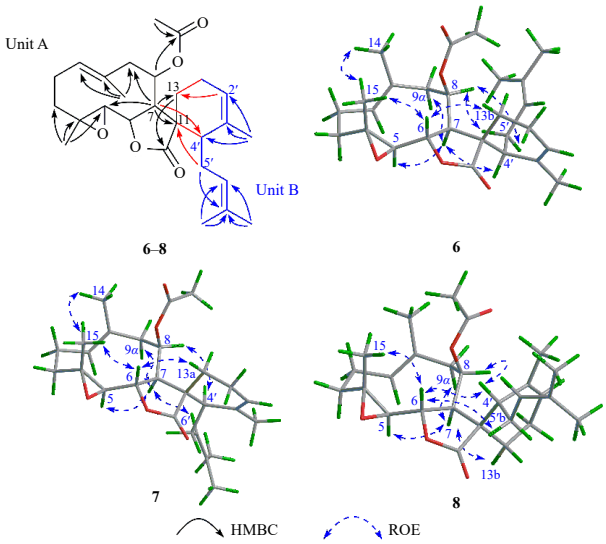

Fig. 5 Selected HMBC and ROESY correlations of **6–8**.

3.2. Plant material

The leaves and branches of *L. chinense* were collected in

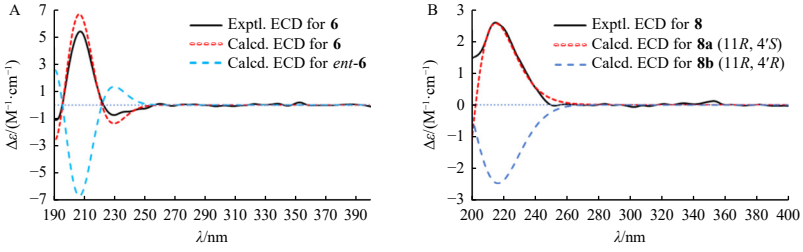

Fig. 6 Experimental and calculated ECD spectra of **6** (A) and **8** (B).

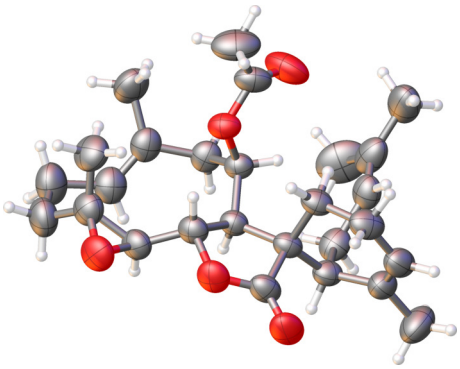

Fig. 7 Olex2 drawing of **6**.

November 2019 and October 2020, respectively, from the campus of Taizhou University, Zhejiang Province, China. The species was identified by Prof. Zexin Jin (Taizhou University, Zhejiang, China), one of the co-authors. The voucher specimens (Nos. 20191113 and 20201020) were deposited at the Department of Natural Medicine, School of Pharmacy at Fudan University.

3.3. Extraction and isolation

The dried branches (13.1 kg) and leaves (6.3 kg) of *L. chinense* were extracted separately with 90% MeOH (12 L × 12 h) at ambient temperature five times. After evaporation of the solvent *in vacuo*, the crude residues (branches: 1.1 kg; leaves: 0.8 kg) were suspended in 3% tartaric acid aqueous solution, then extracted with ethyl acetate (EtOAc) to obtain the non-alkaloid components. The aqueous layer was adjusted to pH 9–10 with Na_2CO_3 followed by a partition with $CHCl_3$ to afford the alkaloid-containing fraction, from which a series of alkaloids and alkaloid-sesquiterpene heterodimers were isolated [6, 7]. Analyses by HPLC and TLC demonstrated that chemical constituents of the two EtOAc extracts from branches and leaves were superimposable, which were subsequently combined (totaling 426.7 g) for further isolation and purification.

The EtOAc partition underwent CC over silica gel (100–200 mesh) with petroleum ether/EtOAc gradients (from 30∶1 to neat EtOAc, *V/V*) to yield seven fractions (Fr. 1–Fr. 7). All fractions were subsequently analyzed by HPLC-PDA-MS with a full scan, revealing that three fractions (Fr. 2, 3 and 5) contained numerous components with distinctive molecular weights (e.g., *m/z* 442, 458, 474) compared to sesquiterpenoid monomers (details shown in Fig. S1). These three fractions were selected for additional purification.

Fr. 2 (11.4 g) underwent fractionation by an MCI column using a gradient MeOH/H_2O (from 50% to 100%, *V/V*) to produce eight subfractions (Fr. 2A–Fr. 2H). Fr. 2D (1.3 g) was separated through CC over silica gel (100–200 mesh, petroleum ether–acetone, 15∶1→0∶1), yielding Fr. 2D-1–Fr. 2D-6. Fr. 2D-2 (0.3 g) underwent further purification by gel permeation chromatography (GPC) over Sephadex LH-20 (MeOH) followed by semi-preparative HPLC, yielding compounds **7** (4.0 mg; XBridge, MeOH–H_2O 80∶20, *V/V*, 3.0 mL·min^{-1}, t_R 15.3 min), **12** (8.1 mg; XBridge, MeOH–H_2O 80∶20, *V/V*, 3.0 mL·min^{-1}, t_R 13.9 min), and **8** (2.7 mg; SB-Phenyl, MeCN–H_2O 75∶25, *V/V*, 3.0 mL·min^{-1}, t_R 9.5 min). Compounds **1** (7.5 mg, t_R 23.1 min) and **3** (3.7 mg, t_R 18.5 min) were obtained from Fr. 2D-5 (75.2 mg) through repeated chromatographic separation on Sephadex LH-20 (MeOH) and semi-preparative HPLC (XBridge, MeOH–H_2O, 68∶32, *V/V*, 2.4 mL·min^{-1}).

Fr. 3 (10.9 g) underwent separation *via* MCI column elution with MeOH–H_2O in a stepwise gradient (from 50% to 100%, *V/V*), yielding seven subfractions (Fr. 3A–Fr. 3G). Compound **2** (1.3 mg, t_R 13.4 min) was isolated from Fr. 3D (4.6 g) through silica gel CC (100–200 mesh, petroleum ether–acetone 40∶1→neat acetone) and semi-preparative HPLC (XBridge, MeOH–H_2O 70∶30, *V/V*, 2.4 mL·min^{-1}). Compound **6** (5.2 mg, t_R 25.0 min) was isolated from Fr. 3F (6.3 g) using silica gel CC (100–200 mesh, petroleum ether–acetone, 30∶1→neat acetone) and semi-preparative HPLC (XBridge, MeOH–H_2O 73∶17, *V/V*, 3.0 mL·min^{-1}). Fr. 3G (0.72 g) was fractionated by silica gel CC (100–200 mesh, petroleum ether–acetone, 40∶1→neat acetone) followed by semi-preparative HPLC to yield compounds **9** (23.6 mg; XBridge, MeCN–H_2O 68∶32, *V/V*, 3.0 mL·min^{-1}, t_R 21.5 min), **10** (28.8 mg; SB-Phenyl, MeCN–H_2O 58∶42, *V/V*, 3.0 mL·min^{-1}, t_R 20.9 min), and **11** (1.7 mg; Sunfire, MeOH–H_2O 72∶28, *V/V*, 3.0 mL·min^{-1}, t_R 27.9 min).

Fr. 5 (20.5 g) underwent fractionation through CC over MCI gel (MeOH–H_2O, from 30% to 100%, *V/V*) yielding five subfractions Fr. 5A–Fr. 5E. Fr. 5D (1.0 g) was fractionated by silica gel (100–200 mesh, from neat CH_2Cl_2 to CH_2Cl_2–MeOH 10∶1) followed by purification using semi-preparative HPLC (Sunfire, MeOH–H_2O 72∶28, *V/V*, 3.0 mL·min^{-1}) to obtain compound **4** (19.6 mg, t_R 17.7 min). Fr. 5E (0.4 g) underwent purification *via* GPC over Sephadex LH-20 (MeOH) and semi-preparative HPLC (XBridge, MeOH–H_2O 68∶32, *V/V*, 3.0 mL·min^{-1}) to yield compound **5** (29.5 mg, t_R 11.2 min).

3.4. Identification of new compounds

Lirispirolide A (**1**): colorless needles (MeOH); $[\alpha]_D^{25}$ −107.0 (*c* 0.34, $CHCl_3$); UV (MeCN) λ_{max} (log ε) 191 (4.59) nm; ECD (*c* 3.46 × 10^{-5} mol·L^{-1}, MeCN) λ_{max} ($\Delta\varepsilon$) 205 (−26.5) nm; ^{1}H and ^{13}C NMR data, see Table 1; (+)-HR-ESI-MS *m/z* 497.2513 [M + Na]$^+$ (Calcd. for $C_{27}H_{38}O_7Na^+$, *m/z* 497.2510).

Lirispirolide B (**2**): white amorphous powder; $[\alpha]_D^{25}$ +52.6 (*c* 0.13, MeOH); UV (MeCN) λ_{max} (log ε) 192 (4.56) nm; ECD (*c* 6.95 × 10^{-5} mol·L^{-1}, MeCN) λ_{max} ($\Delta\varepsilon$) 200 (+23.0) nm; ^{1}H and ^{13}C NMR data, see Table 1; (+)-HR-ESI-MS *m/z* 497.2501 [M + Na]$^+$ (Calcd. for $C_{27}H_{38}O_7Na^+$, *m/z* 497.2510).

A

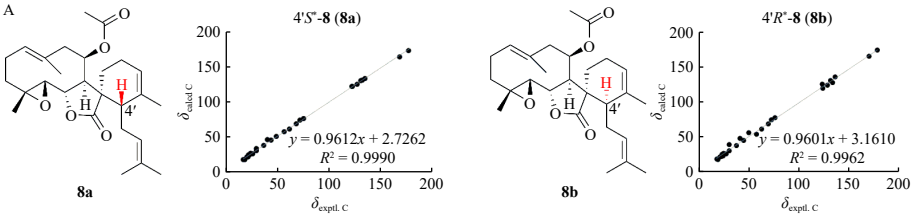

B

	MAE (carbon)	MAE (proton)	CMAE (carbon)	CMAE (proton)	DP4+ (H data)	DP4+ (C data)	DP4+ (all data)
8a (4'*S*)	1.82	0.10	1.22	0.09	100.00%	100.00%	100.00%
8b (4'*R*)	2.59	0.22	2.47	0.21	0.00%	0.00%	0.00%

Fig. 8 (A) Linear correlation plots of calculated versus experimental ^{13}C NMR chemical shifts of **8**. (B) Mean absolute error (MAE), corrected MAE, and DP4+ probability analyses (sarotti-nmr.weebly.com) for **8a** (4'*S**) and **8b** (4'*R**). The PCM/b3lyp/6-31g (d) level of theory was used for NMR calculations.

Table 5 ^{1}H NMR (600 MHz) data for **9**–**12** (*J* in Hz).

No.	**9** [a]	**10** [a]	**11** [a]	**12** [a]	**12** [b]
1	5.32, br d (12.0)	5.32, br d (11.6)	5.34, br d (12.2)	5.31, br d (11.7)	5.40, br d (11.8)
2*α*	2.23, m	2.23, m	2.24, m	2.25, m	2.06, m
2*β*	2.43, dddd (13.0, 12.9, 12.0, 5.9)	2.42, dddd (13.0, 12.7, 11.6, 6.0)	2.41, m	2.40, m	2.30, m
3*α*	1.29, ddd (13.0, 12.9, 6.6)	1.28, ddd (13.1, 12.7, 6.8)	1.29, ddd (12.8, 12.4, 6.9)	1.28, ddd (13.0, 12.4, 7.1)	1.27, ddd (12.9, 12.5, 6.8)
3*β*	2.17, m	2.17, br dd (13.1, 6.0)	2.18, m	2.17, br dd (13.0, 6.2)	2.06, m
5	2.74, d (8.9)	2.74, d (9.3)	2.72, d (9.4)	2.72, d (9.2)	2.99, d (9.3)
6	4.44, dd (8.9, 8.8)	4.44, dd (9.5, 9.3)	4.44, dd (9.5, 9.4)	4.43, dd (9.3, 9.2)	4.81, dd (9.4, 9.3)
7	2.35, br d (8.8)	2.23, br d (9.5)	2.26, br d (9.5)	2.29, br d (9.3)	2.73, br d (9.4)
8	5.53, br d (5.9)	5.20, br d (6.2)	5.14, br d (6.1)	5.27, br d (6.1)	5.52, br d (6.4)
9*α*	2.09, br d (14.2)	2.10, br d (14.1)	2.12, br d (14.1)	2.09, m	2.24, m
9*β*	2.79, dd (14.2, 5.9)	2.81, dd (14.1, 6.2)	2.86, dd (14.1, 6.1)	2.85, dd (14.2, 6.1)	2.93, dd (14.1, 6.4)
13a	1.95, dd (13.4, 12.3)	1.69, m	1.72, m	1.71, m	1.99, m
13b	1.65, m	1.11, dd (12.9, 11.6)	1.41, dd (13.4, 10.6)	1.68, m	1.98, m
14	1.67, br s	1.70, br s	1.69, br s	1.69, br s	1.64, br s
15	1.34, s	1.35, s	1.34, s	1.35, s	1.34, s
8-OAc	2.07, s	2.01, s	2.09, s	2.07, s	2.13, s
1'a	2.29, br d (17.4)	2.12, m	1.95, m	2.43, br d (17.4)	2.59, br d (17.0)
1'b	2.00, br d (17.4)	2.11, m	1.94, m	2.00, m	2.12, br d (17.0)
2'	5.40, br s	5.40, br s	5.24, br s	5.50, br s	5.51, br s
4'	2.03, m	2.22, m	2.98, m	2.01, m	2.18, m
5'a	2.37, m	2.32, br d (15.2)	2.34, m	2.25, m	2.34, m
5'b	2.12, m	1.93, ddd (15.2, 8.1, 7.2)	1.98, ddd (14.9, 7.5, 7.2)	2.02, m	2.19, m
6'	5.03, br dd (7.1, 7.0)	4.93, br dd (7.2, 7.2)	5.06, br dd (7.2, 7.0)	5.00, br dd (7.2, 6.8)	5.12, m
8'	1.62, br s	1.58, br s	1.63, br s	1.60, br s	1.57, br s
9'	1.72, br s	1.68, br s	1.73, d (1.0)	1.70, br s	1.59, br s
10'	1.73, d (1.2)	1.71, br s	1.70, br s	1.74, d (1.2)	1.75, d (1.2)

[a] acquired in $CDCl_3$; [b] acquired in pyridine-d_5.

Lirispirolide C (**3**): white amorphous powder; $[\alpha]_D^{25}$ +94.8 (*c* 0.29, MeOH); UV (MeCN) λ_{max} (log ε) 191 (4.53) nm; ECD (*c* 3.82 × 10^{-5} mol·L^{-1}, MeCN) λ_{max} ($\Delta\varepsilon$) 199 (+27.4) nm; ^{1}H and ^{13}C NMR data, see Table 1; (+)-HR-ESI-MS *m/z* 497.2512 $[M + Na]^+$ (Calcd. for $C_{27}H_{38}O_7Na^+$, *m/z* 497.2510).

Lirispirolide D (**4**): white amorphous powder; $[\alpha]_D^{25}$ −23.0 (*c* 0.30, MeOH); UV (MeCN) λ_{max} (log ε) 192 (4.43) nm; ECD (*c* 8.56 × 10^{-5} mol·L^{-1}, MeCN) λ_{max} ($\Delta\varepsilon$) 204 (−35.3) nm; IR (KBr) ν_{max}: 3455, 2971, 2931, 1770, 1740, 1440, 1384, 1239, 1154, 1110, 1066, 1032, 992, 735 cm^{-1}; ^{1}H and ^{13}C NMR data, see Table 2; (+)-HR-ESI-MS *m/z* 481.2527 $[M + Na]^+$ (Calcd. for $C_{27}H_{38}O_6Na^+$, *m/z* 481.2561).

Lirispirolide E (**5**): white amorphous powder; $[\alpha]_D^{25}$ +62.7 (*c* 0.57, MeOH); UV (MeCN) λ_{max} (log ε) 192 (4.39) nm; ECD (*c* 8.59 × 10^{-5} mol·L^{-1}, MeCN) λ_{max} ($\Delta\varepsilon$) 199 (+33.7) nm; ^{1}H and ^{13}C NMR data, see Table 2; (+)-HR-ESI-MS: *m/z* 481.2558 $[M + Na]^+$ (Calcd. for $C_{27}H_{38}O_6Na^+$, *m/z* 481.2561).

Lirispirolide F (**6**): colorless needles (MeOH), mp: 214–215 °C; $[\alpha]_D^{25}$ +2.4 (*c* 0.60, $CHCl_3$); UV (MeCN) λ_{max} (log ε) 191 (4.27) nm; ECD (*c* 7.47 × 10^{-5} mol·L^{-1}, MeCN) λ_{max} ($\Delta\varepsilon$) 208 (+2.7), 230 (−0.4) nm; IR (KBr) ν_{max}: 2973, 2926, 2861, 1770, 1747, 1442, 1379, 1242, 1065, 1035, 1003, 946, 827, 735 cm^{-1}; ^{1}H and ^{13}C NMR data, see Tables 3 and 4; (+)-HR-ESI-MS *m/z* 465.2595 $[M + Na]^+$ (Calcd. for $C_{27}H_{38}O_5Na^+$, *m/z* 465.2611).

Lirispirolide G (**7**): white amorphous powder; $[\alpha]_D^{25}$ −42.3 (*c* 0.30, MeOH); UV (MeCN) λ_{max} (log ε) 192 (4.28) nm; ECD (*c* 9.37 × 10^{-5} mol·L^{-1}, MeCN) λ_{max} ($\Delta\varepsilon$) 196 (−2.2), 219 (+0.3), 233 (−0.1) nm; ^{1}H and ^{13}C NMR data, see Tables 3 and 4; (+)-HR-ESI-MS *m/z* 465.2598 $[M + Na]^+$ (calcd for $C_{27}H_{38}O_5Na^+$, *m/z* 465.2611).

Lirispirolide H (**8**): white amorphous powder; $[\alpha]_D^{25}$ +58.8 (*c* 0.20, MeOH); UV (MeCN) λ_{max} (log ε) 192 (4.33) nm; ECD (*c* 8.90 × 10^{-5} mol·L^{-1}, MeCN) λ_{max} ($\Delta\varepsilon$) 215 (+2.6) nm; ^{1}H and ^{13}C NMR data, see Tables 3 and 4; (+)-HR-ESI-MS *m/z* 465.2610 $[M + Na]^+$ (Calcd. for $C_{27}H_{38}O_5Na^+$, *m/z* 465.2611).

Lirispirolide I (**9**): colorless needles (MeOH), mp: 155–156 °C; $[\alpha]_D^{25}$ −67.0 (*c* 0.73, $CHCl_3$); UV (MeCN) λ_{max} (log ε) 193 (4.58) nm; ECD (*c* 7.04 × 10^{-5} mol·L^{-1}, MeCN) λ_{max} ($\Delta\varepsilon$) 196 (−16.3) nm; IR (KBr) ν_{max}: 2925, 2858, 1768, 1745, 1441, 1382, 1235, 1035, 1010, 931, 829, 554 cm^{-1}; ^{1}H and ^{13}C NMR data, see Tables 3 and 5; (+)-HR-ESI-MS *m/z* 443.2790 $[M + H]^+$ (Calcd. for $C_{27}H_{39}O_5^+$, *m/z* 443.2792).

Lirispirolide J (**10**): colorless needles (MeOH); $[\alpha]_D^{25}$ −41.0 (*c* 0.80, $CHCl_3$); UV (MeCN) λ_{max} (log ε) 192 (4.34) nm; ECD (*c* 1.21 × 10^{-4} mol·L^{-1}, MeCN) λ_{max} ($\Delta\varepsilon$) 200 (−8.5) nm; ^{1}H and ^{13}C NMR

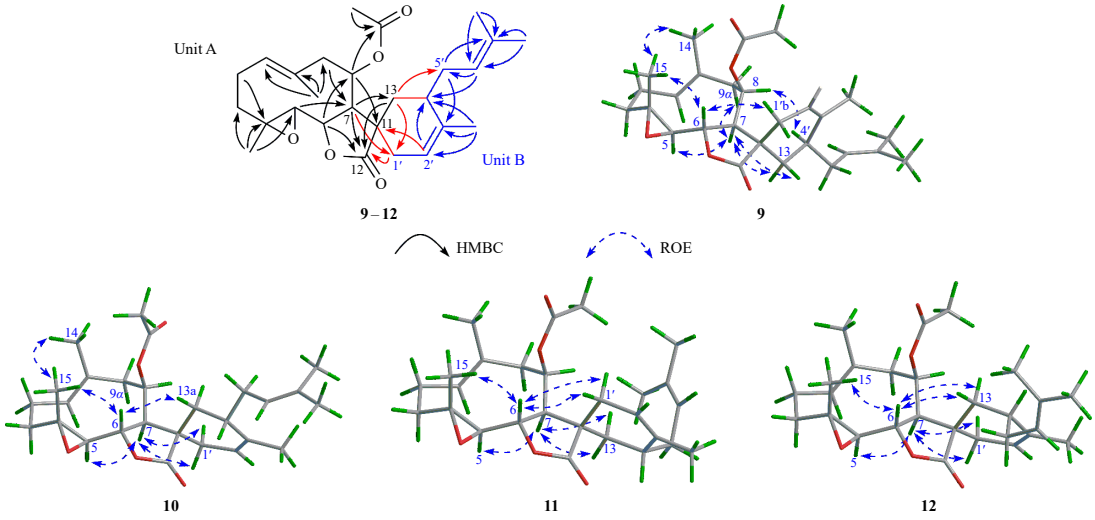

Fig. 9 Key HMBC and ROESY correlations of **9**–**12**.

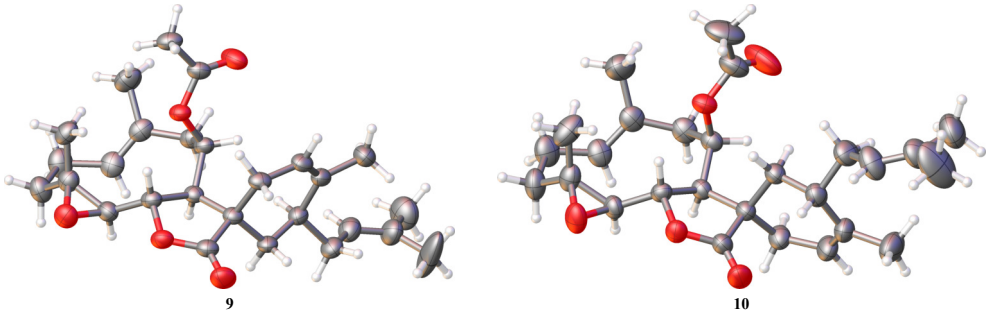

Fig. 10 Olex2 drawing of **9** and **10**.

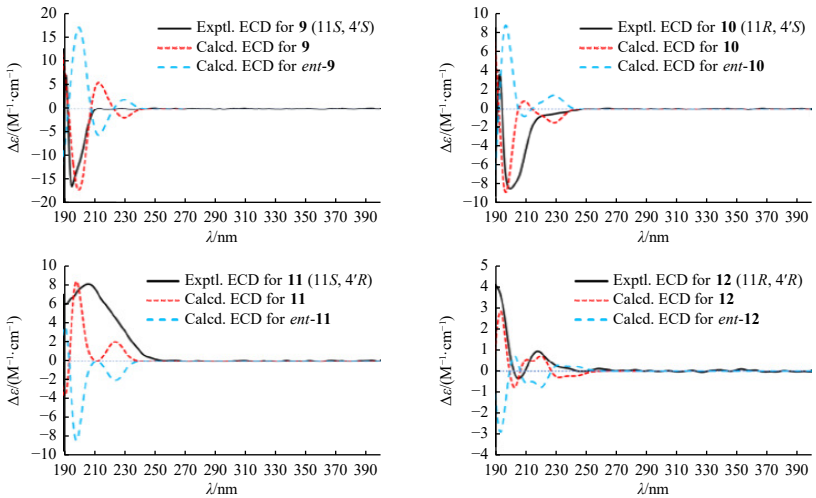

Fig. 11 Experimental and calculated ECD spectra of **9**–**12**.

data, see Tables 3 and 5; (+)-HR-ESI-MS *m/z* 443.2792 $[M + H]^+$ (Calcd. for $C_{27}H_{39}O_5^+$, *m/z* 443.2792).

Lirispirolide K (**11**): white amorphous powder; $[\alpha]_D^{25}$ +5.9 (*c* 0.17, MeOH); UV (MeCN) λ_{max} (log ε) 192 (4.55) nm; ECD (*c* 7.69 × 10^{-5} mol·L^{-1}, MeCN) λ_{max} ($\Delta\varepsilon$) 206 (+8.2) nm; ^1H and ^{13}C NMR data, see Tables 3 and 5; (+)-HR-ESI-MS *m/z* 443.2788 $[M + H]^+$ (Calcd. for $C_{27}H_{39}O_5^+$, *m/z* 443.2792).

Lirispirolide L (**12**): colorless oil; $[\alpha]_D^{25}$ +10.8 (*c* 0.54, MeOH); UV (MeCN) λ_{max} (log ε) 192 (4.55) nm; ECD (*c* 8.99 × 10^{-5} mol·L^{-1}, MeCN) λ_{max} ($\Delta\varepsilon$) 205 (−0.3), 218 (+1.0) nm; ^1H and ^{13}C NMR data, see Tables 3 and 5; (+)-HR-ESI-MS *m/z* 465.2612 $[M + Na]^+$ (Calcd. for $C_{27}H_{38}O_5Na^+$, *m/z* 465.2611).

3.5. Computational calculations of $^1H/^{13}C$ NMR and ECD data

Monte Carlo conformational searches were conducted using Schrodinger 2015 software (Schrödinger, Inc., NY, USA) with the MMFF force field. Conformers with a Boltzmann population exceeding 5% were selected for NMR or ECD calculations and initially optimized at the b3lyp/6-311g (d, p) or b3lyp/6-31g (d) level in gas. NMR calculations were performed using gauge-independent atomic orbital (GIAO) at the b3lyp/6-31g (d) level, and

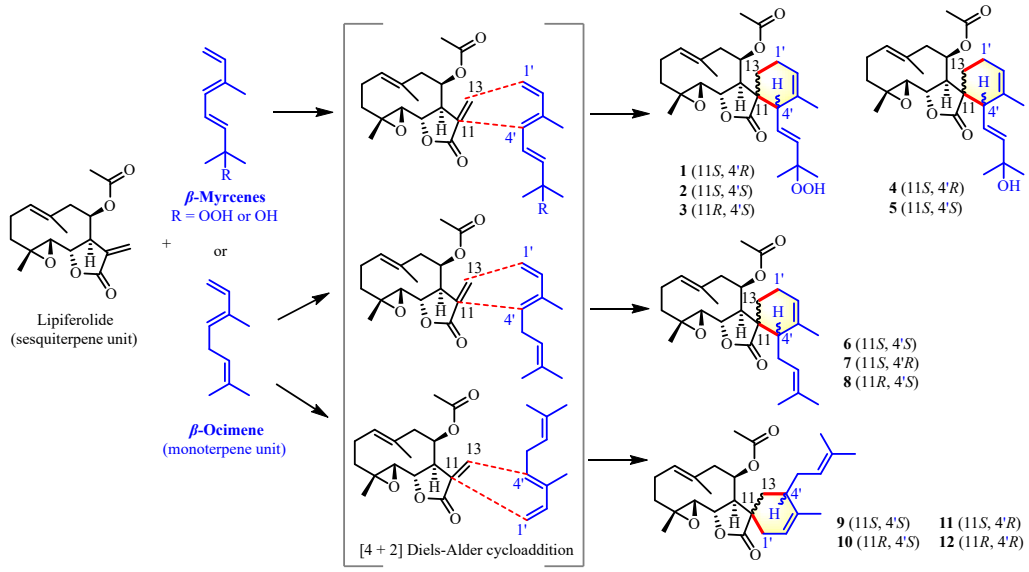

Scheme 1 Proposed biosynthetic pathways for compounds **1**–**12**.

Table 6 Inhibitory effects on LPS-induced NO production in mouse BV-2 cells (mean ± SD, n = 3).

Compound	IC_{50}/(μmol·L^{-1})	Cell viability/% [a]
2	25.19 ± 4.53	84.32 ± 2.16
3	43.41 ± 2.29	94.05 ± 2.30
4	31.24 ± 4.78	91.87 ± 0.96
5	29.84 ± 4.38	93.29 ± 2.02
6	27.85 ± 3.99	92.21 ± 2.12
7	29.30 ± 3.34	73.23 ± 2.88
8	46.70 ± 2.23	87.28 ± 3.00
9	17.10 ± 3.23	78.88 ± 1.62
10	10.84 ± 1.78	97.82 ± 2.00
11	38.01 ± 4.25	94.66 ± 1.97
12	48.14 ± 3.38	76.31 ± 3.30
L-NMMA[b]	14.42 ± 1.23	97.90 ± 4.10

[a] After treatment with 50 μmol·L^{-1} of each tested compound, cell viability is expressed as a percentage (%) of untreated control group; [b] L-NMMA (N^G-monomethyl-L-arginine): positive control.

the calculated shielding constants underwent statistical analyses with DP4+ probability weighted by Boltzmann distribution rate. The theoretical ECD calculation was performed in MeCN using TD-DFT at the b3lyp/6-311g (d, p) level for all compound conformers. Rotatory strengths were calculated for 30 excited states. ECD spectra were generated using SpecDis version 1.6 (University of Würzburg, Würzburg, Germany) from dipole-length rotational strengths by applying Gaussian band shapes with a sigma of 0.3 eV.

*3.6. X-ray crystallographic data of compounds **1**, **6**, **9** and **10***

Single crystals of compounds **1**, **6**, **9**, and **10** were obtained from a MeOH solution at room temperature. The crystal structures were determined through direct methods using SHELXT. Refinements were conducted with SHELXL-2015 (University of Göttingen, Göttingen, Germany) using full-matrix least-squares calculations on F^2, with anisotropic displacement parameters for all non-hydrogen atoms. The hydrogen atom positions were geometrically idealized and allowed to ride on their parent atoms. The crystallographic data have been deposited at the Cambridge Crystallographic Data Centre (CCDC). CCDC 2311480 (**1**), 2311481 (**6**), 2311482 (**9**), and 2311483 (**10**) contain the supplementary crystallographic data, which can be obtained free of charge from the CCDC *via* www.ccdc.cam.ac.uk.

Crystallographic data of **1**: $C_{27}H_{38}O_7$, Mr = 474.57, orthorhombic, space group $P2_12_12_1$, a = 11.7417 (2) Å, b = 14.0633 (2) Å, c = 15.5966 (3) Å, $\alpha = \beta = \gamma$ = 90°, V = 2575.42 (8) Å^3, Z = 4, D_{calcd} = 1.224 Mg·m^{-3}, μ(Ga Kα) = 0.457 mm^{-1}, crystal size 0.07 × 0.06 × 0.05 mm^3, F(000) = 1024, 28897 reflections collected, 4885 independent reflections (R_{int} = 0.0333), R_1 = 0.0276 [$I > 2\sigma(I)$], wR_2 = 0.0726 [$I > 2\sigma(I)$], R_1 = 0.0281 (all data), wR_2 = 0.0729 (all data), Goodness of fit = 1.052, Flack parameter = 0.03 (4).

Crystallographic data of **6**: $C_{27}H_{38}O_5$, Mr = 442.57, orthorhombic, space group $P2_12_12_1$, a = 7.6674 (5) Å, b = 15.0747 (10) Å, c = 22.2441 (16) Å, $\alpha = \beta = \gamma$ = 90°, V = 2571.1 (3) Å^3, Z = 4, D_{calcd} = 1.143 Mg·m^{-3}, μ(Cu Kα) = 0.618 mm^{-1}, crystal size 0.16 × 0.15 × 0.06 mm^3, F(000) = 960, 24849 reflections collected, 4860 independent reflections (R_{int} = 0.1227), R_1 = 0.0746 [$I > 2\sigma(I)$], wR_2 = 0.1750 [$I > 2\sigma(I)$], R_1 = 0.0773 (all data), wR_2 = 0.1808 (all data), Goodness of fit = 1.062, Flack parameter = 0.07 (17).

Crystallographic data of **9**: $C_{27}H_{38}O_5$, Mr = 442.57, monoclinic, space group $P12_11$, a = 13.4830 (6) Å, b = 7.0308 (3) Å, c = 13.9819 (6) Å, $\alpha = \gamma$ = 90°, β = 109.571 (2)°, V = 1248.86 (9) Å^3, Z = 2, D_{calcd} = 1.177 Mg·m^{-3}, μ(Ga Kα) = 0.405 mm^{-1}, crystal size 0.06 × 0.05 × 0.02 mm^3, F(000) = 480, 13827 reflections collected, 4695 independent reflections (R_{int} = 0.0662), R_1 = 0.0479 [$I > 2\sigma(I)$], wR_2 = 0.1295 [$I > 2\sigma(I)$], R_1 = 0.0525 (all data), wR_2 = 0.1352 (all data), Goodness of fit = 1.025, Flack parameter = 0.04 (14).

Crystallographic data of **10**: $C_{27}H_{38}O_5$, Mr = 442.57, orthorhombic, space group $P2_12_12_1$, a = 6.6691 (2) Å, b = 19.2344 (6) Å, c = 19.5711 (6) Å, $\alpha = \beta = \gamma$ = 90°, V = 2510.50 (13) Å^3, Z = 4, D_{calcd} = 1.171 Mg·m^{-3}, μ(Ga Kα) = 0.403 mm^{-1}, crystal size 0.06 × 0.05 × 0.02 mm^3, F(000) = 960, 18374 reflections collected, 4756 independent reflections (R_{int} = 0.0589), R_1 = 0.0429 [$I > 2\sigma(I)$], wR_2 = 0.1002 [$I > 2\sigma(I)$], R_1 = 0.0606 (all data), wR_2 = 0.1125 (all data), Goodness of fit = 1.043, Flack parameter = 0.04 (17).

3.7. Anti-neuroinflammatory assay

The mouse microglia cell line BV-2 was obtained from the

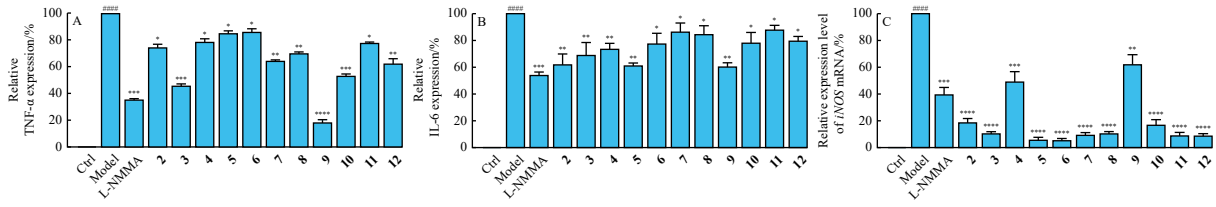

Fig. 12 Inhibitory effects of compounds **2**–**12** on the production of (A) TNF-α, (B) IL-6, and (C) the expression of *iNOS* mRNA in LPS-induced BV-2 microglial cells. Data were expressed as means ± SD (n = 3). $^{\#\#\#\#}P < 0.0001$ *vs* the control group; $^{*}P < 0.05$, $^{**}P < 0.01$, $^{***}P < 0.001$, $^{****}P < 0.0001$ *vs* the model group. Ctrl: control group. The model group was treated with LPS (1 μg·mL^{-1}) for 24 h. L-NMMA was used as the positive control.

National Collection of Authenticated Cell Cultures. Cells were cultured in DMEM (Meilunbio, Dalian, China) supplemented with 10% fetal bovine serum and 1% penicillin/streptomycin. Cells were seeded at a density of 5 × 10^4 cells·mL^{-1} into 96-well plates with 200 μL/well and incubated at 37 °C in a 5% CO_2 incubator (Thermo Fisher, Waltham, MA, USA). The anti-neuroinflammatory activity in BV-2 cells was evaluated according to a reported protocol [45]. NO production was quantified by nitrite accumulation in the culture medium using a Griess reaction kit (Beyotime, Shanghai, China). BV-2 microglial cells were pretreated with a concentration gradient (2.5, 5.0, 10.0, 20.0, 25.0, and 50.0 μmol·L^{-1}) of indicated compounds for 4 h, followed by LPS (1 μg·mL^{-1}, dissolved in ddH_2O) for 24 h. The isolated supernatants (50 μL) were mixed with equal volumes of Griess reagent I and Griess reagent II. NO production was evaluated by measuring optical density at 540 nm using a microplate reader (Thermo Fisher, Waltham, MA, USA). Cell viability was assessed using CCK-8 assay [5]. N^G-monomethyl-L-arginine (L-NMMA, Beyotime, Shanghai, China) served as a positive control.

To evaluate the inhibitory effects of isolates on pro-inflammatory cytokines (IL-6 and TNF-α) and iNOS expression, BV-2 microglial cells were seeded at a density of 3 × 10^5 cells·mL^{-1} in 96-well plates and cultured at 37 °C in a 5% CO_2 incubator. Following 24 h of seeding, cells were pretreated with compounds at their IC_{50} values for 4 h, followed by LPS (1 μg·mL^{-1}) treatment for 24 h. The inhibitory effects on pro-inflammatory cytokines were assessed by analyzing the supernatants using mouse IL-6 enzyme-linked immunosorbent assay (ELISA) kit and mouse TNF-α ELISA kit. For iNOS expression analysis, total RNA was extracted through cell lysis, centrifugation, precipitation, and washing. Subsequently, complementary deoxyribonucleic acid (cDNA) was synthesized using 5 × ABScriptII RT Mix for quantitative polymerase chain reaction (qPCR) (ABclonal, Wuhan, China) with 8 μL total RNA. PCR was conducted using 2 μL cDNA, 10 μL 2 × Universal SYBR Green Fast qPCR Mix (ABclonal, Wuhan, China), 1 μL mouse iNOS forward primer, 1 μL mouse iNOS reverse primer, and 6 μL DEPC water.

Statistical analysis was performed using GraphPad Prism 10.0 (GraphPad Software, Inc., San Diego, CA, USA). The results represent the averages of three independent experiments, with data expressed as mean ± standard deviation (SD).

Funding

This work was supported by the National Natural Science Foundation of China (Nos. 82373752 and 21937002) and the Science and Technology Commission of Shanghai Municipality (No. 22ZR1414400).

Supporting information

Details of NMR calculations and ECD calculations, the crystal data of **1**, **6**, **9** and **10**, the original 1D/2D NMR, UV, and IR spectra along with HR-ESI-MS reports of **1**–**12** can be obtained by contacting the corresponding authors *via* E-mail.

Declaration of competing interest

These authors have no conflict of interest to declare.

References

1 Xia N, Liu Y, Hans PN. *Flora of China*. Beijing: Science Press. 2008;7:48-91.
2 Jiangsu New Medical College. *A Dictionary of the Traditional Chinese Medicine*. Shanghai Science and Technology Press. 1986:1157-1628.
3 Ministry of Ecology and Environment of the People's Republic of China. *List of Red Species of Biodiversity in China: Higher Plants Volume*. 2023-05-19. https://www.mee.gov.cn/xxgk2018/xxgk/xxgk01/202305/t20230522_1030745.html.
4 Cho HM, Park EJ, Park YJ, et al. Sesquiterpene lactone and its unique proaporphine hybrids from *Magnolia grandiflora* L. and their anti-inflammatory activity. *Phytochemistry*. 2022;200:113211. https://doi.org/10.1016/j.phytochem.2022.113211.
5 He YH, Li QX, Wu YF, et al. Liriogerphines A–D, a class of sesquiterpene-alkaloid hybrids from the rare Chinese tulip tree plant. *J Org Chem*. 2022;87(10):6927-6933. https://doi.org/10.1021/acs.joc.2c00318.
6 He YH, Xiang H, Li QX, et al. Liriogerphines E–U, further unique sesquiterpene-alkaloid hybrids from the rare Chinese tulip tree. *Phytochemistry*. 2024;218:13956. https://doi.org/10.1016/j.phytochem.2023.113956.
7 Xu KL, Li C, Li CJ, et al. Oligomeric phenylpropanoids having new skeletons and hypoglycemic activity from *Magnolia officinalis* var. *biloba*. *Org Chem Front*. 2021;8(17):4833-4838. https://doi.org/10.1039/D1QO00795E.
8 Xu KL, Ma J, Li C, et al. P-menthane-based meroterpenoids with neuroprotective effects from the bark of *Magnolia officinalis* var. *biloba*. *Tetrahedron*. 2022;123:132964. https://doi.org/10.1016/j.tet.2022.132964.
9 Li C, Li CJ, Ma J, et al. Magterpenoids A–C, three polycyclic meroterpenoids with PTP1B inhibitory activity from the bark of *Magnolia officinalis* var. *biloba*. *Org Lett*. 2018;20(12):3682-3686. https://doi.org/10.1021/acs.orglett.8b01476.
10 Li C, Li CJ, Ma J, et al. Magmenthanes A–H: eight new meroterpenoids from the bark of *Magnolia officinalis* var. *biloba*. *Bioorg Chem*. 2019;88:102948. https://doi.org/10.1016/j.bioorg.2019.102948.
11 Hu X, Sui X, Wang Y, et al. Sesquiterpene-neolignans from *Manglietia hookeri*. *Nat Prod Res*. 2016;30(13):1477-1483. https://doi.org/10.1080/14786419.2015.1110703.
12 Ninh PT, Ha CTT, Thai TH, et al. Chevalierinol A and B, two new neolignan sesquiterpenoids from *Magnolia chevalieri*. *Nat Prod Res*. 2021;35(21):3745-3751. https://doi.org/10.1080/14786419.2020.1736061.
13 Tietze LF, Bell HP, Chandrasekhar S. Natural product hybrids as new leads for drug discovery. *Angew Chem Int Ed*. 2003;42(34):3996-4028. https://doi.org/10.1002/anie.200200553.
14 Walsh CT, Fischbach MA. Natural products version 2.0: connecting genes to molecules. *J Am Chem Soc*. 2010;132(8):2469-2493. https://doi.org/10.1021/ja909118a.
15 Yang XW, Grossman RB, Xu G. Research progress of polycyclic polyprenylated acylphloroglucinols. *Chem Rev*. 2018;118(7):3508-3558. https://doi.org/10.1021/acs.chemrev.7b00551.
16 Liu B, Fu S, Zhou C. Naturally occurring [4 + 2] type terpenoid dimers: sources, bioactivities and total syntheses. *Nat Prod Rep*. 2020;37(12):1627-1660. https://doi.org/10.1039/C9NP00037B.
17 Wang GQ. *Compilation of Countrywide Herbal Medicine of China*. Vol. II. Beijing: People's Medical Publishing House. 2014.
18 Fu LK, Jin JM. *China Plant Red Data Book. Rare and Endangered Plants I*. Beijing: Science Press. 1992.
19 Phan KL. *Liriodendron chinense. The IUCN Red List of Threatened Species*. 2015:e.T31284A2803363. https://www.iucnredlist.org/species/31284/2803363.
20 National Forestry and Grassland Administration. *List of National Key Protected Wild Plants*. 2021-09-07. https://www.gov.cn/zhengce/zhengceku/2021-09/09/content_5636409.htm.
21 Wu YF, Zhao ZY, Yang MJ, et al. Pentacyclic triterpenoids as potential ACL inhibitors from the rare medicinal plant *Semiliquidambar cathayensis*. *Fitoterapia*. 2024;176:106018. https://doi.org/10.1016/j.fitote.2024.106018.
22 Dong Y, Liang D, Huang JJ, et al. Sesquiterpenes with quinone reductase-inducing activity from *Lirodendron chinense*. *Nat Prod Commun*. 2009;4(4):467-468.
23 Doskotch RW, Jr Keely SL, Hufford CD, et al. New sesquiterpene lactones from *Liriodendron tulipifera*. *Phytochemistry*. 1975;14(3):769-773. https://doi.org/10.1016/0031-9422(75)83032-9.

24 Andersson PG, Bäckvall JE. Synthesis of furanoid terpenes *via* an efficient palladium-catalyzed cyclization of 4,6-dienols. *J Org Chem*. 1991;56(18): 5349-5353. https://doi.org/10.1021/jo00018a027.

25 Rücker G, Mayer R, Manns D. *α*- and *β*-Myrcene hydroperoxide from *Artemisia annua*. *J Nat Prod*. 1987;50(2):287-289. https://doi.org/10.1021/np50050a038.

26 Bruhn T, Schaumloffel A, Hemberger Y, et al. SpecDis: quantifying the comparison of calculated and experimental electronic circular dichroism spectra. *Chirality*. 2013;25(4):243-249. https://doi.org/10.1002/chir.22138.

27 Marcarino MO, Cicetti S, Zanardi MM, et al. A critical review on the use of DP4+ in the structural elucidation of natural products: the good, the bad and the ugly. A practical guide. *Nat Prod Rep*. 2022;39(1):58-76. https://doi.org/10.1039/D1NP00030F.

28 Xiong J, Zhou PJ, Jiang HW, et al. Forrestiacids A and B, pentaterpene inhibitors of ACL and lipogenesis: extending the limits of computational NMR methods in the structure assignment of complex natural products. *Angew Chem Int Ed*. 2021;60(41):22270-22275. https://doi.org/10.1002/anie.202109082.

29 Chen FY, He ML, Xu LL, et al. Lindenane sesquiterpenoid monomers and oligomers: chemistry and pharmacological activities. *Phytochemistry*. 2023;215:113866. https://doi.org/10.1016/j.phytochem.2023.113866.

30 Wang XJ, Xin JL, Xiang H, et al. Holotrichones A and B, potent anti-leukemic lindenane-type sesquiterpene trimers with unprecedented complex carbon skeletons from a rare *Chloranthus* species. *Chin Chem Lett*. 2024;35:109682. https://doi.org/10.1016/j.cclet.2024.109682.

31 Son SR, Kim GJ, Choi YJ, et al. Patriniaterpenes A–D: unveiling the unique structure and antioxidant properties of monoterpene-sesquiterpene conjugates from *Patrinia scabra*. *Org Chem Front*. 2023;10(17):4320-4328. https://doi.org/10.1039/D3QO00835E.

32 Langat MK, Crouch NR, Nuzillard JM, et al. Pseudopulchellol: a unique sesquiterpene-monoterpene derived C-25 terpenoid from the leaves of *Croton pseudopulchellus* Pax (Euphorbiaceae). *Phytochem Lett*. 2018;23:38-40. https://doi.org/10.1016/j.phytol.2017.11.008.

33 Kim JH, Kim HK, Jeon SB, et al. New sesquiterpene-monoterpene lactone, artemisolide, isolated from *Artemisia argyi*. *Tetrahedron Lett*. 2002;43(35): 6205-6208. https://doi.org/10.1016/s0040-4039(02)01315-1.

34 Su BN, Takaishi Y, Tori M, et al. Macrophyllols A and B, two unusual novel sesquiterpene and monoterpene dimers from the bark of *Inula macrophylla*. *Org Lett*. 2000;2(4):493-496. https://doi.org/10.1021/ol990401n.

35 Herz W, Pethtel KD, Raulais D. Isoflavones, a sesquiterpene lactone-monoterpene adduct and other constituents of *Gaillardia* species. *Phytochemistry*. 1991;30(4):1273-1279. https://doi.org/10.1016/s0031-9422(00)95216-6.

36 Bohlmann F, Mathur R, Jakupovic J, et al. Furanoheliangolides and other compounds from *Calea hymenolepis*. *Phytochemistry*. 1982;21(8):2045-2048. https://doi.org/10.1016/0031-9422(82)83040-9.

37 Appendino G, Taglialatela-Scafati O, Romano A, et al. Genepolide, a sesterpene *γ*-lactone with a novel carbon skeleton from mountain wormwood (*Artemisia umbelliformis*). *J Nat Prod*. 2009;72(3):340-344. https://doi.org/10.1021/np800468m.

38 Gao L, Su C, Du X, et al. FAD-dependent enzyme-catalysed intermolecular [4 + 2] cycloaddition in natural product biosynthesis. *Nat Chem*. 2020;12(7): 620-628. https://doi.org/10.1038/s41557-020-0467-7.

39 Candelario-Jalil E, Dijkhuizen RM, Magnus T. Neuroinflammation, stroke, blood-brain barrier dysfunction, and imaging modalities. *Stroke*. 2022;53(5): 1473-1486. https://doi.org/10.1161/STROKEAHA.122.036946.

40 Stuckey SM, Ong LK, Collins-Praino LE, et al. Neuroinflammation as a key driver of secondary neurodegeneration following stroke. *Int J Mol Sci*. 2021; 22(23):13101. https://doi.org/10.3390/ijms222313101.

41 Troubat R, Barone P, Leman S, et al. Neuroinflammation and depression: a review. *Eur J Neurosci*. 2021;53(1):151-171. https://doi.org/10.1111/ejn.14720.

42 Dhapola R, Hota SS, Sarma P, et al. Recent advances in molecular pathways and therapeutic implications targeting neuroinflammation for Alzheimer's disease. *Inflammopharmacology*. 2021;29(6):1669-1681. https://doi.org/10.1007/s10787-021-00889-6.

43 Ibrahim MA, Na M, Oh J, et al. Significance of endangered and threatened plant natural products in the control of human disease. *Proc Natl Acad Sci U S A*. 2013;110(42):16832-16837. https://doi.org/10.1073/pnas.1311528110.

44 Zhu F, Qin C, Tao L, et al. Clustered patterns of species origins of nature-derived drugs and clues for future bioprospecting. *Proc Natl Acad Sci U S A*. 2011;108(31):12943-12948. https://doi.org/10.1073/pnas.1107336108.

45 Wang XJ, Yu SZ, Xin JL, et al. Further terpenoids from the Chloranthaceae plant *Chloranthus multistachys* and their anti-neuroinflammatory activities. *Fitoterapia*. 2022;156:105068. https://doi.org/10.1016/j.fitote.2021.105068.